Atp6v0a4 knockout mouse is a model of distal renal tubular acidosis with hearing loss, with additional extrarenal phenotype

Elizabeth E. Norgett[a,1], Zoe J. Golder[a,1], Beatriz Lorente-Cánovas[b], Neil Ingham[b], Karen P. Steel[b], and Fiona E. Karet Frankl[a,2]

[a]Department of Medical Genetics, University of Cambridge, Cambridge CB2 0XY, United Kingdom; and [b]Wellcome Trust Sanger Institute, Hinxton CB10 1SA, United Kingdom

Edited by Jonathan G. Seidman, Harvard Medical School, Boston, MA, and approved July 10, 2012 (received for review March 15, 2012)

Autosomal recessive distal renal tubular acidosis (dRTA) is a severe disorder of acid–base homeostasis, often accompanied by sensorineural deafness. We and others have previously shown that mutations in the tissue-restricted a4 and B1 subunits of the H^+-ATPase underlie this syndrome. Here, we describe an *Atp6v0a4* knockout mouse, which lacks the a4 subunit. Using β-galactosidase as a reporter for the null gene, developmental a4 expression was detected in developing bone, nose, eye, and skin, in addition to that expected in kidney and inner ear. By the time of weaning, *Atp6v0a4*$^{-/-}$ mice demonstrated severe metabolic acidosis, hypokalemia, and early nephrocalcinosis. Null mice were hypocitraturic, but hypercalciuria was absent. They were severely hearing-impaired, as shown by elevated auditory brainstem response thresholds and absent endocochlear potential. They died rapidly unless alkalinized. If they survived weaning with alkali supplementation, treatment could later be withdrawn, but −/− animals remained acidotic with alkaline urine. They also had an impaired sense of smell. Heterozygous animals were biochemically normal until acid-challenged, when they became more acidotic than +/+ animals. This mouse model recapitulates the loss of H^+-ATPase function seen in human disease and can provide additional insights into dRTA and the physiology of the a4 subunit.

proton pump | distal nephron

Maintenance of systemic pH is essential for many physiological functions. Metabolism and the human omnivorous diet create an excess acid load of about 1 mmol/kg body weight, which must be excreted to maintain appropriate systemic pH. The fine regulation of pH (in humans, to 7.36–7.44) is carried out in the kidney by bicarbonate reclamation in the proximal tubule and a combination of acid excretion and bicarbonate generation in the distal nephron.

H^+ ions are actively excreted in the collecting duct by specialized polarized epithelial cells: α-intercalated cells (α-ICs). Vacuolar-type proton pumps (H^+-ATPases) are found at high density on their α-IC apical (luminal) membrane. Bicarbonate is transported basolaterally by the Cl^-/HCO_3^- exchanger AE1 (anion exchanger 1), which is functionally coupled by an ill-understood mechanism to the apical H^+-ATPase. Protons reaching the collecting duct lead to acidification of urine, the pH of which can in humans vary from 4.5 to 8.5. Urinary bicarbonate secretion and basolateral H^+ movement by oppositely polarized β-ICs are not major functions of the human nephron but may be more important in rodents, given their much more alkaline diet.

All H^+-ATPases consist of two domains: a cytosolic, catalytic V_1 domain (where ATP is hydrolyzed, containing subunits A through H); and a membrane-bound V_0 domain across which proton transfer occurs, and the five subunits of which are a, c, c″, d, and e. All subunits are encoded by separate genes. Generic H^+-ATPases are present in the membranes of intracellular organelles such as endosomes and lysosomes, where acidification is vital. At plasma membrane sites of high H^+-ATPase expression such as osteoclasts in bone, inner-ear epithelia, and clear cells of the epididymis, as well as ICs in kidney, a number of specific individual generic subunits (a1, B2, C1, G1, and d1) are replaced by tissue-restricted ones (a2, a3, a4, B1, C2, G2, G3, d2) (1). To date, there are no known disease-associated mutations affecting generic subunits, but examples of mutations in tissue-restricted subunits include *ATP6V0A2* (encoding the a2 subunit), causing cutis laxa/wrinkly skin syndrome (2); and *ATP6V0A3* (encoding the a3 subunit), causing recessive osteopetrosis (3, 4).

Renal tubular acidosis (RTA), which forms the backdrop to this study, is a heterogeneous condition that can be either proximal (because of impaired bicarbonate reabsorption) or distal (because of functional failure of α-ICs and concomitant impairment of urine acidification). Distal (d)RTA is characterized by normal anion gap metabolic acidosis (overt or compensated) with inappropriately alkaline urine (pH > 5.5 in humans), hypokalemia, hypercalciuria, hypocitraturia, and nephrocalcinosis. It can arise secondary to autoimmune disease such as Sjögren syndrome or can be inherited dominantly or recessively. Dominant dRTA is generally less severe than recessive, and is due to mutations in *SLC4A1*, which encodes AE1 (5). In contrast, recessive (r)dRTA presents in infancy or early childhood, usually with severe spontaneous acidosis accompanied by failure to thrive, growth retardation, and rickets in untreated cases. Many children also display progressive sensorineural hearing loss. We and others have shown that rdRTA can be attributable to destructive mutations in *ATP6V1B1* or *ATP6V0A4*, encoding the B1 and a4 subunits of the H^+-ATPase, respectively (6–8). These subunit forms replace a1 and B2 in plasma membrane pumps in the kidney and ear.

Deafness in dRTA has illustrated the importance of endolymphatic pH homeostasis. Although first reports suggested that *ATP6V1B1* mutations conferred early-onset deafness (6) whereas *ATP6V0A4* mutations did not affect hearing (7), it has become clear that deafness arises in both (8, 9). Widened vestibular aqueducts have also been noted (10).

Atp6v1b1 has been ablated in mice in an attempt to generate a model of dRTA (11), and although this line demonstrated a requirement for the B1 subunit for maximal urinary acidification upon acid challenge, no spontaneous acidosis was observed. Furthermore, *Atp6v1b1*$^{-/-}$ mice had normal hearing (12). Here, we report an *Atp6v0a4*-null line that much more closely resembles the human disease state.

Author contributions: K.P.S. and F.E.K.F. designed research; E.E.N., Z.J.G., B.L.-C., and N.I. performed research; K.P.S. contributed new reagents/analytic tools; E.E.N., Z.J.G., B.L.-C., N.I., K.P.S., and F.E.K.F. analyzed data; and E.E.N., Z.J.G., B.L.-C., N.I., and F.E.K.F. wrote the paper.

The authors declare no conflict of interest.

This article is a PNAS Direct Submission.

Freely available online through the PNAS open access option.

[1]E.E.N. and Z.J.G. contributed equally to this work.

[2]To whom correspondence should be addressed. E-mail: fek1000@cam.ac.uk.

This article contains supporting information online at www.pnas.org/lookup/suppl/doi:10.1073/pnas.1204257109/-/DCSupplemental.

MEDICAL SCIENCES

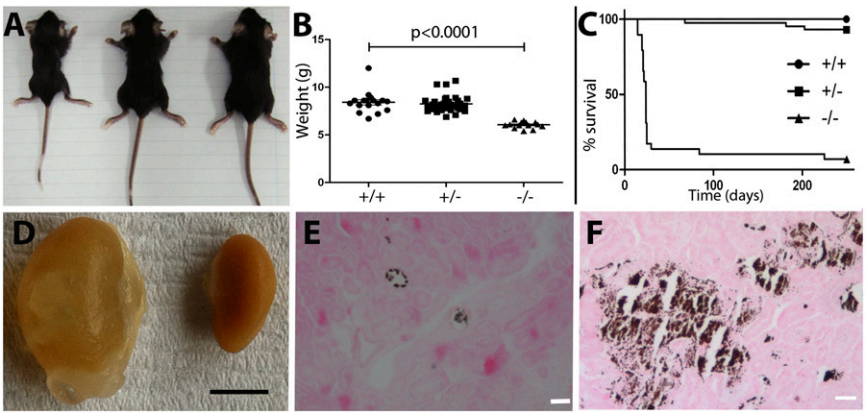

Fig. 1. Gross morphology and survival. Untreated p21 mice: appearance of –/–, +/–, and +/+ respectively, *Left* to *Right* (*A*). (*B*) Weight: –/– animals had significantly lower body weight than +/+ or +/– animals. (*C*) Survival curve over 250 d (+/+ $n = 25$; +/–, $n = 43$; –/–, $n = 29$); only two –/– animals survived until the end of the census period. (*D*) Hydronephrotic kidney from a 9-mo –/– animal (*Left*) in comparison with an age-matched +/+ normal kidney (*Right*). (Scale bar: 5 mm.) Von Kossa staining in a P14 –/– (*E*) and an 8-mo –/– (*F*) animal, showing early and later medullary nephrocalcinosis. (Scale bars: 20 μm.)

Results

Fertility, Gross Morphology, and Survival. Animals generated by breeding founder *Atp6v0a4*$^{+/-}$ stock were genotyped by PCR (Fig. S1*A*), after which the same analysis was applied to all animals. Absence of a4 from *Atp6v0a4*$^{-/-}$ kidneys was confirmed by Western blotting (Fig. S1*B*).

Atp6v0a4$^{+/-}$ × *Atp6v0a4*$^{+/-}$ matings produced live offspring of all three possible genotypes in Mendelian and 1:1 sex ratio (32 +/+, 58 +/–, 30 –/– pups from the first 16 matings). Surviving –/– males and females were fertile, and each produced similar litter sizes to their +/+ and +/– counterparts.

At 2–3 wk, differences were visible between –/– pups and their +/+ and +/– littermates. They were smaller (Fig. 1*A*) and weighed less (Fig. 1*B*). Null mice often staggered, circled, and displayed a head-tilt, consistent with an inner-ear defect. They also lacked a Preyer reflex, suggesting hearing impairment. Around the time of weaning, the vast majority of –/– pups died or had to be killed because of severe ill health. Those that survived usually died suddenly, and almost none lived longer than 6 mo (Fig. 1*C*). Biochemistry, therefore, could not be analyzed in untreated –/– animals older than 21 d.

Seven of 18 kidneys of untreated –/– weanlings examined histologically had mild nephrocalcinosis (Fig. 1*E*). Of the only three long-term survivors, one (died at 8 mo) had marked medullary nephrocalcinosis (Fig. 1*F*) and unilateral hydronephrosis. The latter was also found in the second (7 mo), and the third (9 mo) had severe bilateral hydronephrosis with parenchymal thinning (Fig. 1*D*). One of 71 other untreated –/– animals was also unilaterally hydronephrotic (15 d).

Embryonic Spatial and Temporal Expression of a4 (LacZ). Embryonic day (e)11.5–e18.5 embryos were harvested from heterozygote matings (n = 10–23 from at least two litters per time point). β-Galactosidase (β-gal) activity (driven by the *Atp6v0a4* promoter) was first detected at e12.5 in the developing ear and metanephros, consistent with known localization of a4 protein in adult ear and kidney (Fig. 2 *A*, *D*, and *E*). Adult murine ocular and male reproductive tract a4 expression are also well-recognized; the former was developmentally apparent from e15.5 onwards (Fig. 2*H*). *Atp6v0a4* expression also appeared in the penile urethra from e15.5 (Fig. 2*G*), but, despite the known presence of a4 in narrow and clear cell of the adult epididymis and vas deferens (13, 14), embryonic epididymal expression was not observed.

β-Gal expression was also found at a number of sites not previously associated with a4-containing pumps: developing nose, bones, and skin. It was detectable in nasal cavities from e12.5 onward (Fig. 2 *A* and *B*) and appeared in developing vertebrae, ribs, and long bones from e13.5, moving centrifugally to digits by e16.5 (Fig. 2 *B*, *C*, and *F*). This spatially mirrored the known ossification pattern (15) and was absent in all but the most distal regions by e18.5. Transient expression in epidermis was evident only from e15.5–17.5 (Fig. 2*I*).

Biochemistry. Unweaned –/– animals (P21) had marked spontaneous hyperchloremic non–anion gap acidosis (pH 6.93 ± 0.04; HCO_3 8.8 ± 0.72 mM; base excess (BE) (the amount of acid theoretically required to normalize pH) –23.0 ± 1.00; $P < 0.0001$ for each vs. +/+; all values are means ± SEM (Table 1 and Fig. S2). The –/– animals retained normal excretory renal function but were dehydrated, as evidenced by elevated urea and osmolality. As is the case in dRTA patients, –/– animals were also hypokalemic (K = 2.9 ± 0.14 vs. 3.6 ± 0.08 mM and 3.8 ± 0.05 mM in +/+ or +/– animals; $P < 0.0001$) (Table 1 and Fig. S2). The +/– and +/+ mice were similar for all these parameters.

Auditory Function. Mean auditory brainstem response (ABR) thresholds are shown in Fig. 3*A* for P20 mice; results at P14 were similar. No measurable ABRs were evoked by click stimuli in any of the –/– mice tested, and large elevations in ABR thresholds were seen for click stimuli and all frequencies from 3–42 kHz,

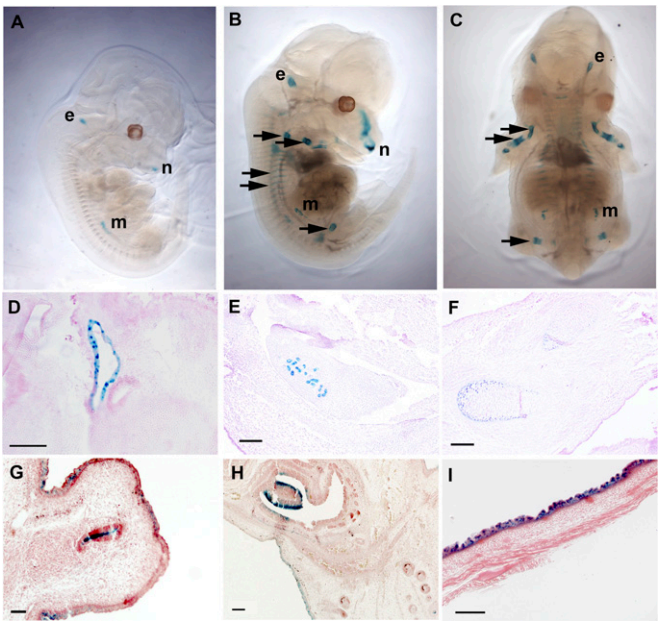

Fig. 2. Embryonic spatial and temporal expression of a4. (*A*) LacZ staining showing *Atp6v0a4* expression in metanephros (m), ear (e), and nasal epithelium (n) in whole-mount embryos at e12.5. (*B* and *C*) Additional expression in developing bone from e13.5 (arrows). (*D–F*) e13.5 embryos. (*D*) Staining is positive in the endolymphatic sac but negative in the cochlea. (*E* and *F*) Positive staining in the metanephros (*E*) and developing long bones in the foreleg (*F*). (*G–I*) e16.5 embryos: expression in the penile urethra (*G*), eye (*H*), and epidermis (*I*). (Scale bars: 100 μm.)

Table 1. Biochemistry of P21 animals

	+/+ (14)	+/− (21)	−/− (11)	*P*
Sodium	142.1 ± 0.43	141.9 ± 0.36	142.8 ± 0.90	NS
Potassium	3.6 ± 0.08	3.8 ± 0.05	2.9 ± 0.14	<0.0001
Chloride	108.9 ± 0.48	109.5 ± 0.59	129.2 ± 1.14	<0.0001
Urea	4.3 ± 0.35	4.8 ± 0.30	12.4 ± 1.28	<0.0001
pH	7.32 ± 0.02	7.32 ± 0.01	6.93 ± 0.04	<0.0001
pCO_2	6.3 ± 0.24	6.6 ± 0.21	5.1 ± 0.22	0.0014
Bicarbonate	23.7 ± 0.43	24.9 ± 0.50	8.8 ± 0.72	<0.0001
Osmolality	289.9 ± 0.54	289.4 ± 0.59	294.3 ± 1.66	0.0116
BE	−2.4 ± 0.59	−1.2 ± 0.50	−23.0 ± 1.00	<0.0001
Creatinine	31.0 ± 3.00*	31.1 ± 2.07†	26.0 ± 2.08*	NS

All values are means ± SEM. *P* values relate to the difference between +/+ and −/−. Numbers of animals are in parentheses. All units are mM, except pCO_2 (kPa); osmolality (mOsm); creatinine (μM); pH; and BE. +/− values were not different from +/+.
*n = 3.
†n = 15.

indicating severely impaired hearing. Fig. 3*B* illustrates the concomitant abolition of endocochlear potentials (EPs) in −/− animals. Cochlear and endolymphatic duct dilatation and a lack of otoconial crystals were also evident (Fig. 3 *C*–*F*). We noted that despite their deafness, maternal behavior of −/− females appeared unimpaired.

Dietary Manipulation and Subsequent Biochemistry. To facilitate survival of *Atp6v0a4*$^{-/-}$ pups to adulthood, drinking water of dams and their litters was alkalinized. Using this regimen, mean weights of mice of all genotypes were similar at 1 and 3 mo. For further analysis, alkali was withdrawn at varying ages from 5 wk to 2.5 mo. Thereafter, −/− animals remained ostensibly healthy and were less acidotic (Table 2) at 3 mo: pH 7.25 ± 0.02 (P = 0.025 vs. +/+); HCO_3 19.3 ± 0.90 [not significant (NS) vs. +/+]; BE −8.0 ± 1.02 (NS vs. +/+). Potassium levels were higher at 3 mo than at 3 wk but remained lower in −/− animals. These data indicate that if they could be supported through the early severe acidotic period, the −/− phenotype stabilized. However, some animals still failed to thrive, suffered rapid weight loss and either died or had to be killed within 14 d of alkali withdrawal.

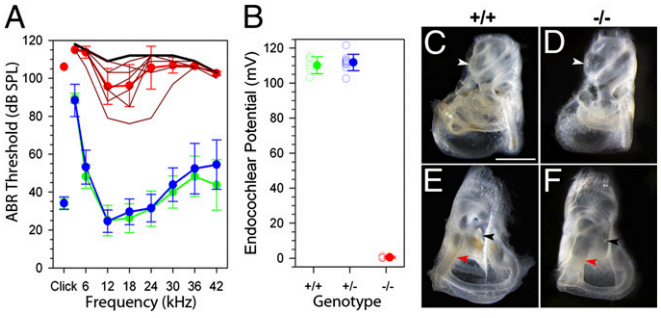

Fig. 3. Auditory function. (*A*) Mean (± SD) ABR thresholds are plotted for +/+ (green; n = 5), +/− (blue; n = 20), and −/− (red; n = 9) mice at P20. Dark lines indicate pure-tone ABR thresholds for individual homozygotes. The black line indicates the maximum output of the sound delivery system at each stimulus frequency. (*B*) EPs recorded from +/+ (green; n = 5), +/− (blue; n = 11), and −/− (red; n = 5) mice at P19–P21. Open symbols indicate measurements from individual animals. Filled symbols indicate mean ± SD for each genotype. (*C*–*F*) Gross morphology of the inner ear at P20 after clearing with glycerol. Front and back views from +/+ (*C* and *E*) and −/− (*D* and *F*) mice are shown. In the mutants, the cochlear duct is expanded compared with controls (*C* and *D*) (white arrowheads). Their endolymphatic ducts are abnormally enlarged (*E* and *F*) (red arrowheads), with a lack of visible otoconial crystals in the mutants (black arrowheads). (Scale bar, 500 μm.)

Urine of surviving adult animals was alkaline following treatment withdrawal (Table 2): pH 7.61 ± 0.09 (−/−) compared with pH 6.54 ± 0.05 (+/−) and pH 6.55 ± 0.06 (+/+) (P < 0.0001). Importantly, in response to their acidosis, marked hypocitraturia was also evident in these −/− animals (citrate: creatinine ratio: 0.1 ± 0.02 compared with 8.4 ± 1.77 in +/+ animals; P = 0.0094). This mirrors the proximal tubular upregulation of citrate reabsorption found in humans with dRTA. Dehydration was less marked in this subgroup: urea and osmolality were more similar. The −/− mice were polyuric but also drank more. Although hypercalciuria is a common feature of human dRTA, urinary and serum calcium and serum phosphate were similar in all genotypes.

Animals receiving continuing alkali supplementation exhibited appropriate biochemical alterations (Table 2 and Table S1). Importantly, biochemistry of −/− animals normalized with this treatment. Strikingly, hydronephrosis was found in 20% (19 of 94) of −/− alkalinized animals, killed at a variety of ages. Only a single animal displayed accompanying hydroureter, suggesting pelviureteric junction obstruction in the rest. There was no evidence of nephrolithiasis in hydronephrotic animals, except one that harbored a very large bladder stone, which surprisingly was composed of struvite. Only two of 169 heterozygotes were hydronephrotic, and no renal tract abnormalities were found in 127 +/+ mice, indicating unlikelihood of spontaneous hydronephrosis in C57BL/6 mice.

Acute or Chronic Acid Challenge. Following acute dosing with NH_4Cl, nadir pH was reached after 2 h (Fig. S3). All three genotypes showed a substantial decrease in pH; this was no more pronounced in −/− animals than +/+ or +/− (Table S2). The +/+ and +/− animals were subjected to chronic acidification for a minimum of 2 wk (Table 3 and Table S3). Similar treatment of null animals was not approved by the licensing authority. As expected, +/+ animals developed a mild acidosis (pH 7.28 ± 0.03; HCO_3 18.5 ± 0.80 mM; pCO_2 5.3 ± 0.36; BE −8.4 ± 1.02), whereas +/− animals became more acidotic (pH 7.16 ± 0.02; HCO_3 15.5 ± 0.83 mM; BE, −13.3 ± 1.21; P = 0.0078, P = 0.0225, and P = 0.008, respectively, vs. +/+), indicating impaired ability of heterozygotes to excrete an excess acid load. The similar urine pH of both groups (pH 5.76 ± 0.07 and pH 5.62 ± 0.06) probably reflects the minimum for this strain.

Histology. Tubular vacuolation was found in six of six untreated P14 and P21 −/− kidneys examined histologically, but not in age-matched +/+ or +/− kidneys (Fig. 4 *A* and *E*). None was seen in lifelong-alkalinized animals, in line with the improvement in −/− biochemistry, but it was seen following treatment withdrawal (three of five). Similar vacuolation was observed in +/+ animals subjected to both acute and chronic acid loading.

The typical α-IC plasma membrane accentuation of H^+-ATPases in +/+ kidneys was replaced by diffuse intracellular localization in *Atp6v0a4*$^{-/-}$ animals (Fig. 4 *B*, *C*, *F*, and *G*). In addition, apical pendrin localization decreased in −/− kidneys (Fig. 4 *D* and *H*). The a4 subunit has been reported subapically in proximal tubule in mouse but not human kidney (7, 16). However, we did not observe proximal tubular a4 in WT mice of this strain, and retinol binding protein (RBP) was not detected by Western blot in undiluted urine of any genotype, whereas it was clearly detectable in 1:10 dilutions of urine from *Clcn5*$^{-/-}$ mice (gift from Thomas Jentsch, Leibniz Institute, Berlin), which have a proximal tubulopathy (17) (Fig. S4).

Histological examination of coronal nasal sections of p5 +/+ animals revealed a4 at the apical pole of cells in olfactory epithelium and the vomeronasal organ (Fig. 5).

Olfactory Behavioral Testing. Using urine of a nonfamiliar animal of the opposite sex as an olfactory discrimination assay, we saw that sexually naïve +/+ mice first approached urine in preference to water (12/14 animals), whereas −/− animals had no preference (3/11; P = 0.005), suggesting hypoosmia.

Table 2. Biochemistry of 3-mo animals

	Untreated*				Chronically alkalinized†				P (−/− untreated vs. −/− alkalinized)
	+/+ (21)	+/− (16)	−/− (23)	P	+/+ (8)	+/− (8)	−/− (9)	P	
Sodium	143.1 ± 0.33	142.3 ± 0.38	144.1 ± 0.39	NS	142.1 ± 0.40	142.8 ± 0.37	142.3 ± 0.44	NS	0.0143
Potassium	4.6 ± 0.17	4.6 ± 0.20	3.8 ± 0.07	0.0002	4.5 ± 0.23	4.4 ± 0.32	4.2 ± 0.12	NS	0.0045
Chloride	112.7 ± 0.45	112.4 ± 0.56	117.3 ± 0.75	<0.0001	112.4 ± 0.57	110.6 ± 0.78	109.6 ± 0.60	0.0041	<0.0001
Urea	7.0 ± 0.34	7.6 ± 0.45	8.5 ± 0.37	0.0038	8.1 ± 0.35	7.0 ± 0.32	7.1 ± 0.33	NS	0.0349
Creatinine	27.3 ± 1.37	25.8 ± 1.85	28.0 ± 1.59 (22)	NS	22.1 ± 2.18	24.0 ± 2.92	25.9 ± 1.36 (8)	NS	NS
Calcium	2.3 ± 0.04 (3)	ND	2.2 ± 0.01 (3)	NS	ND	ND	ND		
Phosphate	1.9 ± 0.17 (3)	ND	2.1 ± 0.15 (3)	NS	ND	ND	ND		
pH	7.31 ± 0. 02	7.31 ± 0. 03	7.25 ± 0.02	0.0248	7.41 ± 0.02	7.33 ± 0.03	7.37 ± 0.03	NS	0.001
pCO_2	5.4 ± 0.24	6.0 ± 0.32	5.9 ± 0.26	NS	4.6 ± 0.38	5.8 ± 0.31	6.2 ± 0.47	0.0185	NS
Bicarbonate	20.3 ± 0.59	22.5 ± 0.82	19.3 ± 0.90	NS	21.4 ± 0.99	23.0 ± 1.29	26.7 ± 0.84	0.0010	<0.0001
Osmolality	298.0 ± 0.61	296.1 ± 0.76 (15)	300.1 ± 0.79	0.0414	296.6 ± 1.07	296.5 ± 0.57	296.6 ± 0.80	NS	0.0136
BE	−6.0 ± 0.75	−3.6 ± 1.12	−8.0 ± 1.02	NS	−1.4 ± 1.15	−2.9 ± 1.62	1.3 ± 0.87	NS	<0.0001
Urine pH	6.55 ± 0.06 (18)	6.54 ± 0.05 (10)	7.61 ± 0.09 (8)	<0.0001	7.51 ± 0.14 (6)	7.78 ± 0.08 (5)	8.55 ± 0.10 (7)	<0.0001	<0.0001
24h urine output	4.3 ± 0.52 (18)	5.8 ± 0.80 (16)	7.2 ± 1.05 (16)	0.0211	6.3 ± 1.08 (12)	4.3 ± 0.68 (10)	8.9 ± 1.65 (14)	NS	NS
24h water intake	9.4 ± 1.02 (18)	10.4 ± 0.92 (16)	13.5 ± 1.56 (16)	0.0426	12.9 ± 1.99 (12)	10.6 ± 0.21 (10)	17.6 ± 2.11 (14)	NS	NS
Urine calcium/Cr ratio	0.9 ± 0.05 (10)	0.9 ± 0.17 (12)	0.7 ± 0.08 (12)	NS					
Urine citrate/Cr ratio	8.4 ± 1.77 (6)	ND	0.1 ± 0.02 (6)	0.0094					

All values are means ± SEM. Numbers of animals are in parentheses. *P* values relate to the difference between +/+ and −/− except in far right column. All units are mM, except pCO_2 (kPa); osmolality (mOsm); creatinine (μM); water intake/urine output (mL); pH; and BE. Cr, creatinine; ND, not determined.

*−/− animals withdrawn from alkali treatment at least 7 d before sample collection.

†−/− animals had received lifelong alkali treatment.

Table 3. Biochemistry of chronically acidified 3-mo animals

	+/+ (*n* = 8)	+/− (*n* = 8)	*P*
Sodium	144.0 ± 0.65	144.3 ± 0.45	NS
Potassium	5.0 ± 0.29	4.4 ± 0.09	NS
Chloride	116.1 ± 1.06	119.9 ± 0.83	0.0147
Urea	7.4 ± 0.54	8.6 ± 0.50	NS
Creatinine	23.6 ± 1.45	22.1 ± 1.55	NS
pH	7.28 ± 0.03	7.16 ± 0.02	0.0078
pCO_2	5.3 ± 0.36	5.8 ± 0.16	NS
Bicarbonate	18.5 ± 0.80	15.5 ± 0.83	0.0225
Osmolality	299.1 ± 1.23	300.3 ± 0.98	NS
BE	−8.4 ± 1.02	−13.3 ± 1.21	0.008
Urine pH	5.76 ± 0.07*	5.62 ± 0.06*	NS
24-h urine output	2.8 ± 0.60*	3.0 ± 0.22*	NS
24-h water intake	7.7 ± 0.98*	7.3 ± 0.68*	NS

All values are means ± SEM. All units are mM, except pCO_2 (kPa); osmolality (mOsm); creatinine (μM); water intake/urine output (mL); pH and BE. *n = 18.

Bone Densitometry. Bone mineral density (BMD) was similar in untreated animals of all three genotypes at 14 and 21 d (Fig. S5 *A* and *B*). Insufficient older untreated −/− animals were available for further analysis. In C57BL/6J mice, BMD increases gradually throughout adulthood and is similar in males and females after 2 mo (18). In chronically acid-dosed adults, we found significantly lower BMD in +/− than +/+ animals at 6 and 9 mo ($P = 0.029$ and $P = 0.028$, respectively; Fig. S5*C*), reflecting their impaired compensatory biochemical mechanisms.

Discussion

This *Atp6v0a4*-null line provides a model for human recessive dRTA, and provides insights into the wider physiology and function of the H^+-ATPase. The biochemical abnormalities in these animals closely resemble those of recessive dRTA patients, including hyperchloremic hypokalemic acidosis with hypocitraturia, illustrating the vital role of *Atp6v0a4* in acid–base homeostasis. In humans, provision of alkali treatment from a young age reverses many of the features of the disorder, as seen here. For *Atp6v0a4*$^{-/-}$ animals surviving weaning, some amelioration of acidosis was observed even following treatment withdrawal. This speaks to the known continuing maturation of the distal nephron postpartum in mice and is also interesting because patients with rdRTA can usually have their treatment reduced as they get older (19). In humans, this is often attributed to achievement of skeletal maturation.

This model does show some notable discrepancies from human dRTA, such as the very early severity of hearing loss. This is worse than that observed in most patients, where some develop late-onset deafness, and in some, hearing is preserved until adulthood (8). The −/− animals lacked the highly positive EP required for normal auditory function and generated by active pumping of K^+ into the scala media by the stria vascularis (20). This loss of endolymphatic homeostasis underlies the importance of proton transport outside, as well as within, the kidney.

Atp6v0a4 expression in the embryonic kidney was detected earlier in gestation than has been reported previously (21), possibly because of differential methodology. Loss of the early expression detected in developing ear is likely to have resulted in the gross anatomical and functional abnormalities found in *Atp6v0a4*$^{-/-}$ animals. Expression of a4 in the developing eye is consistent with known localization in adult mouse pigmented epithelial cells of the retina and ciliary bodies (22). In contrast, although the presence of H^+-ATPase has previously been reported in penile urethra in rat (23), a4 was not sought as a subunit at this site.

Although the role of the a3 subunit of the proton pump in bone resorption by mature osteoclasts is well-established, we have shown previously that the a4 subunit is not expressed in

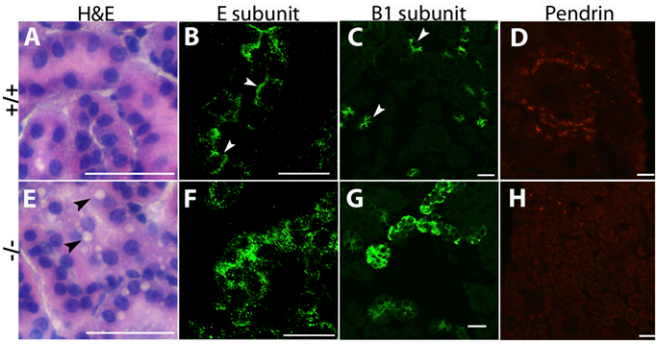

Fig. 4. Histology and immunofluorescence of P21 kidney sections. (*A* and *E*) +/+ (*A*) and –/– (*E*) H&E-stained renal cortex. Tubular vacuolation is evident in the –/– section (black arrows). Normal plasma membrane accentuation of H^+-ATPases in +/+ collecting duct cells is observed with E1 (also present intracellularly in generic H^+-ATPases) and B1 subunit stains (*B* and *C*) (white arrows). This is absent in –/– kidney (*F* and *G*). Normal pendrin staining (*D*) is not seen in $^{-/-}$ section (*H*). (Scale bars: 20 μm.)

adult mouse bone (16). The embryonic expression of *Atp6v0a4* described here did not persist, and the mirroring of ossification pattern suggests that a4 may be involved in early bone modeling/remodelling. a4 expression has also not been reported previously in skin, although the H^+-ATPase d2 subunit (also found in α-IC plasma membrane pumps) has previously been described in Langerhans cells in human adult epidermis (24). By e18.5, epidermal a4 expression was no longer detectable, suggesting that maintenance of skin integrity, in which a2 is known to be important (2), does not involve a4.

The nose was another unexpected site of a4 expression. Păunescu et al. had reported previously the presence of the B1 subunit in olfactory epithelia and vomeronasal organs of mice, suggesting a role in mucosal pH homeostasis and signal transduction and possible similarity of these pumps to those of the α-IC (25). However, olfaction was not functionally assessed in the B1 knockout mouse (11). Unlike *Atp6v0a4*$^{+/+}$ animals, which exhibited a clear preference for a social odor, A*tp6v0a4*$^{-/-}$ animals had no preference for that over water, suggesting hypoosmia and consistent with a role for a4-containing proton pumps in normal olfaction. We also observed that *Atp6v0a4*$^{-/-}$ males are less aggressive in group-housed environments than *Atp6v0a4*$^{+/+}$ males, which could be explained by an abrogated/reduced ability to perceive odors that cause aggressive or territorial behavior. Taken together, these observations highlight the importance of pH regulation in olfaction. Further clinical studies will be needed to assess this in humans but, for practical reasons, fall outside the scope of this report.

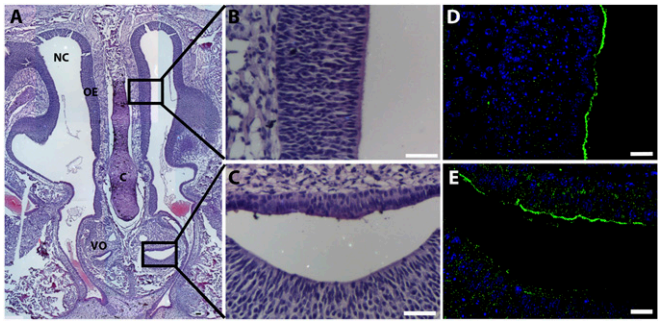

Fig. 5. Histology and immunofluorescence of +/+ p5 nasal tissue. (*A*) H&E-stained coronal section of nasal airway showing nasal cavity (NC), olfactory epithelium (OE), septal cartilage (C), and vomeronasal organ (VO). (*B* and *C*) H&E high-power images of olfactory epithelium and vomeronasal organ. (*D* and *E*) Apical cellular localization of the a4 subunit in respective adjacent sections stained with a4 antiserum. (Scale bars: 20 μm.)

Another feature not noted previously in humans was the reduced compensatory ability of +/– animals to respond to chronically induced acidosis. This was accompanied by lower BMD in heterozygotes, which again emphasizes the importance of pH homeostasis for efficient function at sites distant to the kidney. This is potentially clinically important in the context of human *ATP6V0A4* mutation carriers, especially because the human omnivorous diet results in an acid load. We hypothesize that these carriers may be at higher risk of metabolic bone disease than the general population, and if this is borne out by clinical studies, early detection in these individuals could lead to earlier treatment.

Renal tubular epithelial vacuolation was unsurprising, because it is commonly observed during metabolic stress, being thought to counteract cellular pH changes and protect from damage (26). In contrast, the absence of hypercalciuria in the face of the other manifestations of dRTA was unexpected. Although a definitive explanation for this difference from human disease is not apparent, it was notable that bone was also less affected than in humans, possibly suggesting less calcium mobilization. The absence of significant nephrolithiasis presumably reflects this normocalciuria. The (nonacidotic) *Atp6v1b1*$^{-/-}$ mouse was reported to be relatively hypocalciuric (11), but it is not clear that urine was acidified before analysis in that study. We noted an increase in measured urine calcium of up to 100% between "raw" and acidified aliquots of the same urine (Table S4).

The *Atp6v0a4*-null line more closely resembles human rdRTA than does the *Atp6v1b1*$^{-/-}$ line in a number of respects. This could in part be attributable to differing genetic backgrounds: the *Atp6v1b1* knockout was on a mixed background, whereas this line is pure C57BL/6J. It could also be attributable to different compensatory mechanisms during embryogenesis and the early postnatal period. For example, the B2 subunit of the H^+-ATPase might compensate for loss of B1 better than any of the other "a" subunits can for a4. The creation of this strain also opens the possibility of developing and testing more tailored therapies, or means to ameliorate or prevent hearing impairment, which remains an irreversible feature of dRTA.

Materials and Methods

Generation and Maintenance of *Atp6v0a4*-Deficient Mice. A targeting construct, generated by Ozgene Pty from C57BL/6 genomic DNA, replaced exons 2–4 of *Atp6v0a4* with nuclear localizing signal-β-gal coding sequence downstream of an ATG start codon (Fig. S1*C*). The targeting construct was electroporated into Bruce-4 ES cells. Chimeric mice were back-crossed to Rosa-cre C57BL/6. Male offspring were mated with WT C57BL/6 females; resulting cre-negative animals were used as founders. Genotyping was performed by PCR of genomic DNA from ear biopsies. (*Atp6v0a4* primers: CAAATGTGAACAGCTTCCAGAGG/AGCATCCTTCTCAGGCACTTGG; *LacZ* CGTCTCGTTGCTGCATAAACCG/GCAGGATATCCTGCACCATCG.) Animals were maintained on standard chow and tap water unless otherwise stated. All procedures conformed to the 1986 UK Home Office Animals Scientific Procedures Act. The –/– animals (except those analyzed at p21) received lifelong treatment with 0.14 M $NaHC0_3$/2% (wt/vol) sucrose until adulthood, when some groups ceased this treatment. Some –/– animals of both sexes were mated to assess fertility and maternal behavior.

Whole-Mount Embryo Staining. e11.5–e18.5 embryos from *Atp6v0a4* +/– matings were fixed in 4% (vol/vol) formaldehyde, 2 mM $MgCl_2$, 0.02% Nonidet P-40; e14.5–18.5 embryos were decapitated and epidermis was split before fixing. Embryos were washed [0.1 M phosphate buffer (pH 7.3) containing 2 mM $MgCl_2$, 0.01% Nonidet P-40, 0.02% sodium deoxycholate] and stained overnight in buffer containing 1 mg/mL X-gal, 5 mM potassium ferrocyanide, and 5 mM potassium ferricyanide. Postfixation in 4% formaldehyde preceded storage in 70% (vol/vol) ethanol. Embryos were cleared in KOH/glycerol before photography using a Nikon SMZ1000 microscope and Nikon Digital Sight DS-Fi1 camera.

Western Blot Analysis. Kidney protein lysates were prepared as described previously (7). A total of 20 μg lysate or mouse urine was subjected to SDS/

PAGE and Western blot. Primary antibodies used were anti-a4 for kidney lysates [RA2922; as described previously (7)] and anti-RBP (BD Transduction Laboratories) for urine.

Morphologic and Histologic Analysis and Immunofluorescence. After examining gross anatomy, fresh postmortem tissues or X-Gal–stained embryos were formalin-fixed, paraffin-embedded, and sectioned. After deparaffinization and rehydration, staining with 0.1% neutral red (embryos) and hematoxylin/eosin (H&E) (other tissues) was performed. Von Kossa stain was counterstained with eosin. Images were acquired using a Zeiss Axioskop2 microscope.

Primary antibodies for immunolocalization were RA2922 (1:1,000), α-B1 (1:2,000; gift from G.-H. Sunwada, Doshisha Women's College, Kyoto, Japan), and α-pendrin (1:25; gift from M. Soleimani, Division of Nephrology, University of Cincinnati, Cincinnati, OH) following citrate buffer antigen retrieval and α-E1 (1:100; gift from M. Reuveni, Agricultural Research Organization, Bet Dagan, Israel) following proteinase K antigen retrieval. Sections were examined using a Zeiss LSM510 confocal microscope.

Biochemical Analysis. At p21, untreated animals were terminally anesthetized with isoflurane and arterial blood collected by cardiac puncture. Biochemical parameters were immediately measured using an i-STAT portable clinical analyzer (Abbott). Osmolality was calculated [(1.86 × sodium) + urea + glucose + 9] (Dimension RXL instruction manual; Siemens) and serum creatinine measured (Dimension RXL analyzer; Siemens). Older animals were similarly handled except that alkali supplements were withdrawn from –/– animals at least 7 d before assessment. Stone analysis and urine citrate quantification were performed by the Department of Clinical Biochemistry, University College London Hospitals.

Chronic Dosing with Oral Acid or Alkali. Groups of +/+ and +/– animals were maintained on standard chow until 2.5 mo, after which drinking water was supplemented with either 0.14 M $NaHC0_3$/2% (wt/vol) sucrose, 0.28 M NH_4Cl/2% sucrose, or 2% sucrose alone. After an average 17-d treatment, pairs of age-, sex-, and genotype-matched animals were transferred to metabolic cages (Tecniplast), and water intake and urine output were measured over 24 h. Urinary calcium was measured after acidification with HCl. On exit from metabolic cages, some animals were anesthetized and blood collected as above.

Acute Oral Acid or Alkali Challenge. Groups of animals of each genotype were gavage-fed either water, 0.28 M NH_4Cl or $NaHC0_3$ (0.8 g/kg in a maximum volume of 10 mL/kg). The –/– animals had alkali supplementation withdrawn 7 d prior. Animals were terminally anesthetized at varying time points for blood analysis.

ABR and EP Measurements. ABRs were recorded at 14 and 20 d, as described previously (27). Averaged responses to 256 stimuli presented at 42.2/s were analyzed, and thresholds were established as the lowest sound intensity giving a visually detectable ABR response. EP was recorded in urethane-anesthetized mice aged 19–21 d, as described previously (28), and recorded as the potential difference between the scala media and a reference silver/silver chloride pellet under the neck skin of the animal.

Inner-Ear Clearing. Half-heads were fixed in 75% (vol/vol) ethanol, 5% (vol/vol) formalin, and 5% (vol/vol) glacial acetic acid for 60–120 min, washed in H_2O, then placed in 70% (vol/vol) ethanol for 24 h. Soft tissues were cleared in 3% (vol/vol) KOH for 3–4 d. Specimens were placed in glycerol, 70% ethanol, and benzyl alcohol (2:2:1) for the final stage of clearing and stored in 1:1 glycerol and 70% ethanol.

Bone Mineral Density. BMD of cadavers was measured by dual energy X-ray absorptiometry (DEXA) scanning using a Lunar PIXImus densitometer (GE Medical Systems).

Olfactory Assessment. Sexually naïve animals were transferred singly into a clean cage with two 1-mL syringes hanging, although the top bars. One contained urine from a nonfamiliar animal of opposite sex and the other water. The syringe that the animal approached first with its nose being 1 cm or closer to the tip was recorded.

Statistical Analyses. Significance of difference between –/– and +/+ was tested by unpaired *t* test or χ^2 test as appropriate. Possible heterozygote phenotypes were assessed by examining ratios, and their confidence intervals, of mean differences between –/– and +/– to –/– and +/+.

ACKNOWLEDGMENTS. We thank Keith Burling, Janice Carter, Nick Mudd, Gill Rumsby, Paul Schofield, and Helen Westby for analyses and technical assistance; Thomas Jentsch for *Clcn5*$^{-/-}$ mouse urine; Ge-Hong Sunwada, Moshe Reuveni, and Manoocher Soleimani for antisera; and David Clayton for statistical advice. Ozgene Pty generated the knockout construct. This work was funded by Wellcome Trust Awards 079895, 088489, and 098051 and the Medical Research Council.

1. Smith AN, Borthwick KJ, Karet FE (2002) Molecular cloning and characterization of novel tissue-specific isoforms of the human vacuolar H(+)-ATPase C, G and d subunits, and their evaluation in autosomal recessive distal renal tubular acidosis. *Gene* 297: 169–177.
2. Kornak U, et al.; ARCL Debré-type Study Group (2008) Impaired glycosylation and cutis laxa caused by mutations in the vesicular H+-ATPase subunit ATP6V0A2. *Nat Genet* 40:32–34.
3. Frattini A, et al. (2000) Defects in TCIRG1 subunit of the vacuolar proton pump are responsible for a subset of human autosomal recessive osteopetrosis. *Nat Genet* 25: 343–346.
4. Kornak U, et al. (2000) Mutations in the a3 subunit of the vacuolar H(+)-ATPase cause infantile malignant osteopetrosis. *Hum Mol Genet* 9:2059–2063.
5. Karet FE, et al. (1998) Mutations in the chloride-bicarbonate exchanger gene AE1 cause autosomal dominant but not autosomal recessive distal renal tubular acidosis. *Proc Natl Acad Sci USA* 95:6337–6342.
6. Karet FE, et al. (1999) Mutations in the gene encoding B1 subunit of H+-ATPase cause renal tubular acidosis with sensorineural deafness. *Nat Genet* 21:84–90.
7. Smith AN, et al. (2000) Mutations in ATP6N1B, encoding a new kidney vacuolar proton pump 116-kD subunit, cause recessive distal renal tubular acidosis with preserved hearing. *Nat Genet* 26:71–75.
8. Stover EH, et al. (2002) Novel ATP6V1B1 and ATP6V0A4 mutations in autosomal recessive distal renal tubular acidosis with new evidence for hearing loss. *J Med Genet* 39:796–803.
9. Vargas-Poussou R, et al. (2006) Genetic investigation of autosomal recessive distal renal tubular acidosis: Evidence for early sensorineural hearing loss associated with mutations in the ATP6V0A4 gene. *J Am Soc Nephrol* 17:1437–1443.
10. Andreucci E, et al. (2009) Inner ear abnormalities in four patients with dRTA and SNHL: clinical and genetic heterogeneity. *Pediatr Nephrol* 24:2147–2153.
11. Finberg KE, et al. (2005) The B1-subunit of the H(+) ATPase is required for maximal urinary acidification. *Proc Natl Acad Sci USA* 102:13616–13621.
12. Dou H, Finberg K, Cardell EL, Lifton R, Choo D (2003) Mice lacking the B1 subunit of H+ -ATPase have normal hearing. *Hear Res* 180:76–84.
13. Breton S, Smith PJ, Lui B, Brown D (1996) Acidification of the male reproductive tract by a proton pumping (H+)-ATPase. *Nat Med* 2:470–472.
14. Brown D, Lui B, Gluck S, Sabolić I (1992) A plasma membrane proton ATPase in specialized cells of rat epididymis. *Am J Physiol* 263:C913–C916.
15. Patton JT, Kaufman MH (1995) The timing of ossification of the limb bones, and growth rates of various long bones of the fore and hind limbs of the prenatal and early postnatal laboratory mouse. *J Anat* 186:175–185.
16. Smith AN, et al. (2001) Molecular cloning and characterization of Atp6n1b: A novel fourth murine vacuolar H+-ATPase a-subunit gene. *J Biol Chem* 276:42382–42388.
17. Piwon N, Günther W, Schwake M, Bösl MR, Jentsch TJ (2000) ClC-5 Cl- -channel disruption impairs endocytosis in a mouse model for Dent's disease. *Nature* 408:369–373.
18. Glatt V, Canalis E, Stadmeyer L, Bouxsein ML (2007) Age-related changes in trabecular architecture differ in female and male C57BL/6J mice. *J Bone Miner Res* 22:1197–1207.
19. Soriano JR (2002) Renal tubular acidosis: The clinical entity. *J Am Soc Nephrol* 3: 2160–2170.
20. Tasaki I, Spyropoulos CS (1959) Stria vascularis as source of endocochlear potential. *J Neurophysiol* 22:149–155.
21. Jouret F, et al. (2005) Ubiquitous and kidney-specific subunits of vacuolar H+-ATPase are differentially expressed during nephrogenesis. *J Am Soc Nephrol* 16:3235–3246.
22. Kawamura N, Tabata H, Sun-Wada GH, Wada Y (2010) Optic nerve compression and retinal degeneration in Tcirg1 mutant mice lacking the vacuolar-type H-ATPase a3 subunit. *PLoS ONE* 5:e12086.
23. Herak-Kramberger CM, Breton S, Brown D, Kraus O, Sabolic I (2001) Distribution of the vacuolar H+ atpase along the rat and human male reproductive tract. *Biol Reprod* 64:1699–1707.
24. Sato K, et al. (2006) Selective expression of vacuolar H+-ATPase subunit d2 by particular subsets of dendritic cells among leukocytes. *Mol Immunol* 43:1443–1453.
25. Păunescu TG, Jones AC, Tyszkowski R, Brown D (2008) V-ATPase expression in the mouse olfactory epithelium. *Am J Physiol Cell Physiol* 295:C923–C930.
26. Yang WC, Strasser FF, Pomerat CM (1965) Mechanism of drug-induced vacuolization in tissue culture. *Exp Cell Res* 38:495–506.
27. Ingham NJ, Pearson S, Steel KP (2011) Using the auditory brainstem response (ABR) to determine sensitivity of hearing in mutant mice. *Curr Protoc Mouse Biol* 1:279–287.
28. Steel KP, Barkway C (1989) Another role for melanocytes: Their importance for normal stria vascularis development in the mammalian inner ear. *Development* 107: 453–463.